

Impacts of Perfluoroalkyl Substances on Aqueous and Nonaqueous Phase Liquid Dechlorination by Sulfidized Nanoscale Zerovalent Iron

Du Chen, Xiaohong Hu, Chaohuang Chen, Yiman Gao, Qianhai Zhou, Xia Feng, Xinhua Xu, Daohui Lin, and Jiang Xu*



Cite This: *Environ. Sci. Technol.* 2024, 58, 11193–11202



Read Online

ACCESS |

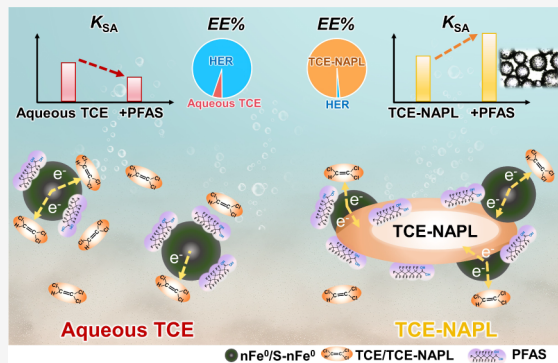
Metrics & More

Article Recommendations

Supporting Information

ABSTRACT: Per- and poly fluoroalkyl substances (PFASs) are often encountered with nonaqueous phase liquid (NAPL) in the groundwater at fire-fighting and military training sites. However, it is unclear how PFASs affect the dechlorination performance of sulfidized nanoscale zerovalent iron (S-nFe^0), which is an emerging promising NAPL remediation agent. Here, S-nFe^0 synthesized with controllable S speciation (FeS or FeS_2) were characterized to assess their interactions with PFASs and their dechlorination performance for trichloroethylene NAPL (TCE-NAPL). Surface-adsorbed PFASs blocked materials' reactive sites and inhibited aqueous TCE dechlorination. In contrast, PFASs-adsorbed particles with improved hydrophobicity tended to enrich at the NAPL–water interface, and the reactive sites were re-exposed after the PFASs accumulation into the NAPL phase to accelerate dechlorination. This PFASs-induced phenomenon allowed the materials to present a higher reactivity (up to 1.8-fold) with a high electron efficiency (up to 99%) for TCE-NAPL dechlorination. Moreover, $\text{nFe}^0\text{-FeS}_2$ with a higher hydrophobicity was more readily enriched at the NAPL–water interface and more reactive and selective than $\text{nFe}^0\text{-FeS}$, regardless of coexisting PFASs. These results unveil that a small amount of yet previously overlooked coexisting PFASs can favor selective reductions of TCE-NAPL by S-nFe^0 , highlighting the importance of materials hydrophobicity and transportation induced by S and PFASs for NAPL remediation.

KEYWORDS: PFASs, chlorinated solvent, hydrophobicity, selective dechlorination, groundwater remediation



1. INTRODUCTION

The co-occurrence of chlorinated solvents and per-/poly fluoroalkyl substances (PFASs) in groundwater and soil often occurs at fire-fighting and military sites, where aqueous film-forming foams (AFFFs) have been widely applied.^{1–4} In general, AFFFs contain various fluorocarbons (e.g., PFASs, to promote foam dispersion and fire asphyxiation) and hydrocarbons, which are discharged into the groundwater along with fuel components and chlorinated solvents during fire suppression.^{5,6} Therefore, PFASs have been globally detected in water and soil, including the sites that use chlorinated solvents. The concentrations of PFASs at these sites range from ng L^{-1} to mg L^{-1} , and chlorinated solvents are often present as nonaqueous phase liquid (NAPL) when discharged into groundwater.^{7–11} This cocontamination has existed since people began to use them but was not discovered until the beginning of this century due to the limitations in analytical instruments for PFASs in the past. And because of their toxicity, persistence, and bioaccumulation,^{12,13} there is an urgent need to develop new materials for efficient remediation.

The unique surface activity of PFASs makes it easy to accumulate at the fluid–fluid interface, e.g., NAPL–water interfaces or even being partitioned into the bulk NAPL phase.^{14–17} This distribution leads to an increase in the retention of PFASs, and the accumulated PFASs can reduce the NAPL–water interfacial tensions and affect the NAPL dissolution.¹⁸ The distribution of PFASs largely depends on characteristics of PFASs and NAPL, e.g., PFASs molecular structure and NAPL saturation.^{15,16,19} Aqueous trichloroethylene (TCE) may inhibit or slightly enhance the adsorption of perfluorooctanesulfonic acid (PFOS) and perfluorooctanoic acid (PFOA) onto colloidal activated carbon, respectively.²⁰ These results suggest that the concentrations and molecular structures of coexisting PFASs could affect the degradation of

Received: May 6, 2024

Revised: June 3, 2024

Accepted: June 5, 2024

Published: June 11, 2024



aqueous TCE and TCE-NAPL by nanoscale zerovalent iron ($n\text{Fe}^0$), which is a widely accepted groundwater remediation agent.^{21–23} However, the impacts of coexisting PFASs on the dechlorination performance of iron materials remains unclear.

Sulfidized nanoscale zerovalent iron ($S\text{-}n\text{Fe}^0$) has been recognized as a better version than $n\text{Fe}^0$ for groundwater remediation.^{24–31} Sulfidation can alter the physicochemical properties of $n\text{Fe}^0$ particles (e.g., accelerated electron transfer, increased hydrophobicity, and inhibited H adsorption) by changing their geometric and electronic structure, thereby improving the materials' performance for contaminant reductions.^{32–35} The reactivity and selectivity of $S\text{-}n\text{Fe}^0$ with TCE could be increased to 3–54 times and 9–160 times higher than those of $n\text{Fe}^0$, respectively.^{32,36,37} Both S content and S speciation are crucial factors that determine the structure–property–activity relationships of materials, and S speciation plays a more significant role in the hydrophobicity of materials compared to S content.^{32,36,38,39} Meanwhile, PFASs could be adsorbed by $n\text{Fe}^0$ and $S\text{-}n\text{Fe}^0$ through hydrophobic and electrostatic interactions, which were affected by the properties of PFASs and the surface corrosion products of $n\text{Fe}^0$ particles.⁴⁰ However, it is unclear how coexisting PFASs affect TCE degradation by $S\text{-}n\text{Fe}^0$ or if S speciation could change this effect. Moreover, TCE contaminations at the source areas with coexisting PFASs often exist as NAPL, serving as a long-term source of TCE in groundwater. Stoichiometric electron excess conditions that represent the remediation scenarios of dissolved TCE in contaminant plumes have been widely studied,^{41–43} but there is limited mechanistic information about the degradation of TCE-NAPL by $S\text{-}n\text{Fe}^0$,⁴⁴ especially in the presence of PFASs. Understanding the influence of PFASs on the performance of $S\text{-}n\text{Fe}^0$ for both aqueous TCE and TCE-NAPL degradation will advance our rational design of materials for specific but important scenarios.

In this work, $n\text{Fe}^0$ and $S\text{-}n\text{Fe}^0$ materials with controllable S speciation (mainly FeS or FeS_2) were synthesized and characterized to assess how S speciation and coexisting PFASs influence the materials' performance for aqueous TCE and TCE-NAPL degradation. Two typical PFASs (PFOA and PFOS) were selected as the probes to understand the impacts of PFASs on their distribution, materials accumulation, and TCE degradation. The results will provide valuable information and an in-depth understanding of the effects of ubiquitous PFASs on the in situ remediation of TCE-contaminated groundwater by $S\text{-}n\text{Fe}^0$ and promote the rational design of materials for emerging, specific, and important scenarios.

2. MATERIALS AND METHODS

2.1. Chemicals. The chemicals used in this study are described in [Text S1](#).

2.2. Synthesis of $n\text{Fe}^0$ and $S\text{-}n\text{Fe}^0$. Unmodified $n\text{Fe}^0$ and $S\text{-}n\text{Fe}^0$ particles with controllable S speciation were prepared according to a reported one-step method.^{32,36} Briefly, 200 mL of 34 g L⁻¹ NaBH_4 and a certain amount of $\text{Na}_2\text{S}\cdot 9\text{H}_2\text{O}$ (or $\text{Na}_2\text{S}_2\text{O}_4$) was dropwise added into a FeCl_3 solution under continuous stirring (350 rpm) and nitrogen purging (0.4 L min⁻¹). The dosed NaBH_4/Fe molar ratio was 5, and the dosed S/Fe molar ratios were 0 and 0.14, respectively. The resulting particles were rapidly washed, magnetically separated, and vacuum-dried at 60 °C for 8 h. The vacuum was released

over 2 h to stabilize the particles before they were sealed and stored in an anaerobic glovebox.

2.3. Batch Experiments. The batch reactivity experiments were conducted in 170 mL serum bottles containing 100 mL of solution and 70 mL of headspace. Overall, two typical scenarios for the coexistence of TCE-NAPL or aqueous TCE with PFASs in groundwater were considered, representing common cocontamination sites near and relatively far from the source, respectively. Since the concentration of PFASs was generally around 100 $\mu\text{g L}^{-1}$ in the AFFFs-impacted groundwater,^{1,2} where chlorinated solvents may coexist, this concentration of PFOA or PFOS was used to probe their potential impacts on the TCE degradation. For the aqueous TCE scenario, the initial TCE concentration in the reaction bottle was ~70 μM and the iron materials were 1.0 g L⁻¹. The simulation of TCE-NAPL scenario was according to previous work,⁴⁴ 100 μL of pure TCE was injected into 100 mL of deionized water, along with the injection of 1 mL PFASs stock solution (10 mg L⁻¹), and equilibrated to form a TCE-NAPL phase along with 100 $\mu\text{g L}^{-1}$ PFASs. Subsequently, 0.1 g of iron materials was added to the bottle to initiate the TCE-NAPL degradation. In all experiments, deoxygenated deionized (DI) water after 1 h of N_2 purging was used, the bottles were capped by Teflon Mininert valves, and the initial pH was 6.0 ± 0.2 and rotated on an end-overend rotator (40 rpm) for 8 days at 25 ± 2 °C. The impacts of S speciation and coexisting PFASs on the mass transfer of materials are described in detail in [Text S2](#).

To assess the performance of iron materials under environmentally relevant conditions, the reactivity and selectivity of materials with TCE were also monitored in real groundwater sampled from a well in Hangzhou, China. Corresponding physicochemical parameters are summarized in [Table S1](#). The detailed experimental process was the same as for the above batch experiments.

2.4. Characterizations. The Fe^0 content was calculated by measuring the generated H_2 after the acidification of ~15 mg of each iron material in 10 mL of HCl. The actual S/Fe molar ratio of each iron material was determined by inductively coupled plasma-optical emission spectroscopy (ICP-OES, ICP6000, Thermo Fisher Scientific, USA) after 10 mL aqua regia digestion of ~15 mg material for 5 h. Brunauer–Emmett–Teller (BET) analysis (MicroActive ASAP 2460, USA) was applied to obtain the specific surface area of the iron materials.

The morphology and the localized elemental distributions of $n\text{Fe}^0$ and $S\text{-}n\text{Fe}^0$ particles were characterized by high-angle annular dark-field scanning transmission electron microscopy (HAADF-STEM, Talos F200X, Thermo Fisher Scientific, USA) coupled with energy-dispersive X-ray spectrometry (EDX, FEI Super X, USA). The crystalline structure of iron materials was analyzed by X-ray diffraction (XRD, Bruker D8 Advance with Cu K α radiation source, Germany) in the 2 θ range of 5–90°. X-ray absorption fine structure (XAFS) spectroscopy was carried out to understand the coordination environment of materials, and details are shown in [Text S3](#). Electrochemical impedance spectroscopy (EIS) and water contact angle (WCA) of iron materials were performed to assess materials' physicochemical properties ([Text S3](#)).

2.5. Analytical Methods. H_2 , TCE, and its degradation products in the headspace were analyzed using a gas chromatograph with thermal conductivity and flame ionization detectors ([Text S4](#)). Aqueous concentrations of TCE

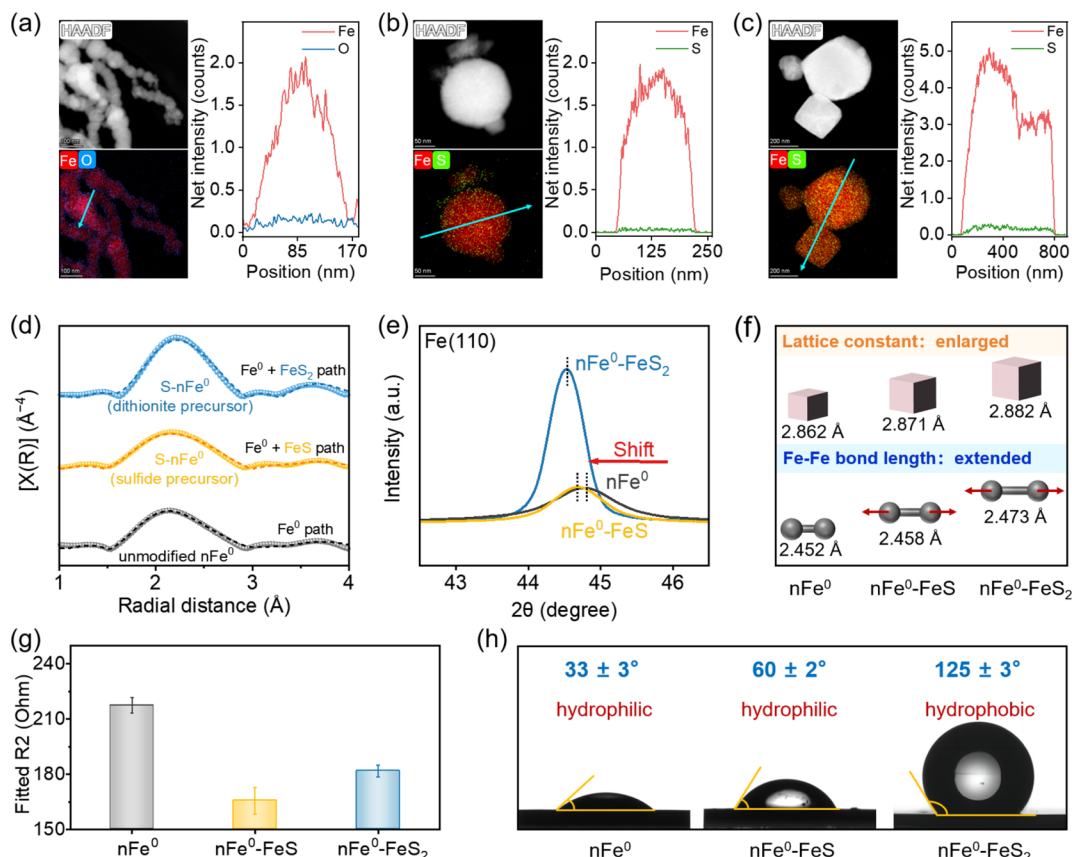


Figure 1. HAADF images and elemental distributions of (a) unmodified $n\text{Fe}^0$, (b) S- $n\text{Fe}^0$ synthesized with a sulfide precursor, and (c) S- $n\text{Fe}^0$ synthesized with a dithionite precursor. (d) Radial structure function of Fe K-edge EXAFS spectra (spherical markers) and their shell fits (dashed lines). (e) XRD patterns of the dominant Fe peak for different materials. (f) Lattice constant of the Fe^0 BCC structure calculated from XRD patterns and Fe-Fe bond length fitted from Fe K-edge EXAFS spectra. (g) Fitted resistance of EIS data and (h) water contact angle of pellets made from materials.

dechlorination products were calculated according to their Henry's law constant to obtain their total concentrations in the reactors (Table S2). Due to the presence of TCE-NAPL and the use of stoichiometrically limited amounts of iron materials compared to TCE, the change in headspace TCE concentration during the TCE degradation experiments was minimal. Thus, the degradation of TCE-NAPL was calculated by quantifying TCE degradation products with time.⁴⁵ Since the contributions of C3–C6 products to the total TCE degradation were minor under these conditions (e.g., < 10% and <1% for aqueous TCE and TCE-NAPL, respectively), they were not considered during the product proportion analysis. The selectivity is defined as the fraction of the Fe^0 electron equivalent used to reduce TCE, which was evaluated by calculating the electron efficiency.⁴⁶ The electron efficiency of iron material for aqueous TCE and TCE-NAPL degradation was calculated after 90% elimination of TCE and 8 days of degradation, respectively. The details of PFASs analysis in the solution and on the materials are provided in Text S5.

To determine the significance of the difference, SPSS 17.0 software was used to do an analysis of variance (ANOVA) and least-significant difference (LSD) between different material treatment outcomes. A confidence level of $p < 0.05$ was defined as significant.

3. RESULTS AND DISCUSSION

3.1. Particle Characterizations. Unmodified $n\text{Fe}^0$ exhibited a typical chain-like structure of spherical nanoparticles with an oxidized shell, and impregnating sulfur into the particles increased the primary particle size (Figures 1a–c and S1). Compared to the materials synthesized with sulfide precursor, the materials synthesized with dithionite precursor shows a relatively stronger intensity on the HAADF images (Figure 1b,c), a higher intraparticle coexistence probability of Fe and S on the elemental maps (Figure S1f,j), and a higher Fe^0 content (80% vs 62%), despite their $[\text{S}/\text{Fe}]_{\text{measured}}$ being close (i.e., 0.06). These discrepancies may reflect varied nucleation process and S speciation and indicate that the latter material could possess a more even S distribution and a higher reduction capability than the former version as discussed later. The improved shell fits of Fe K-edge EXAFS spectra by adding Fe–S scattering paths from mackinawite (FeS) and pyrite (FeS_2) (Figure 1d and Table S3) suggest that the S speciation of S- $n\text{Fe}^0$ materials synthesized with sulfide and dithionite precursors was primary FeS and FeS_2 , respectively.^{34,36} Consistent with the EXAFS results, the Fe^0 peak shifts in the XRD patterns (Figures 1e and S2) indicate that the S impregnation changed the Fe^0 body-centered cubic (BCC) structure, illustrating varied crystallinities and lattice expansion after the incorporation of different S species (Figure 1f).

This modulated geometric structure could affect materials' physicochemical properties. Electrochemical impedance spec-

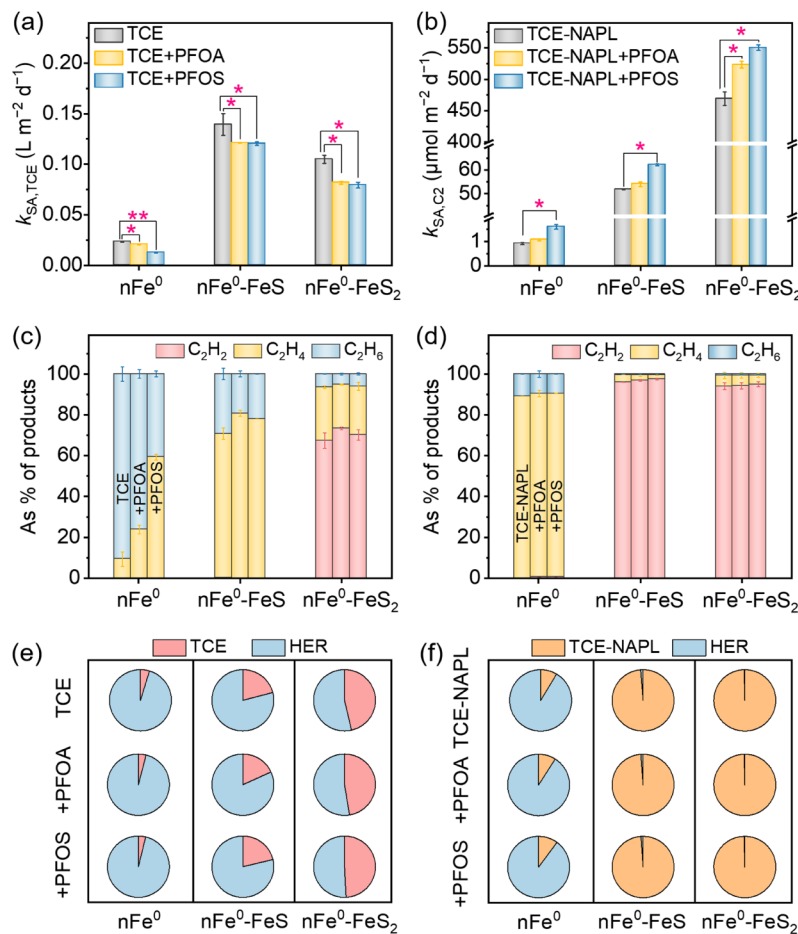


Figure 2. Impacts of S speciation and coexisting PFASs on the (a and b) reactivity, (c and d) product distribution, and (e and f) selectivity of materials for degradations of aqueous TCE and TCE-NAPL (basic conditions: initial pH = 6.0 ± 0.2, T = 25 ± 2 °C, coexisting PFOA or PFOS = 100 $\mu\text{g L}^{-1}$, iron material = 1.0 g L^{-1}).

troscopy (EIS) and its Nyquist curve fits (Figures 1g and S3) show that the S-nFe⁰ materials provided a lower charger transfer resistance (i.e., faster electron transfer) compared to unmodified nFe⁰. This was probably due to the expanded lattice and a lower band gap of iron sulfides than iron oxides, and the lower band gap of FeS than FeS₂ allows nFe⁰-FeS to have lower charge transfer resistance than nFe⁰-FeS₂.^{47,48} In addition, the nFe⁰-FeS₂ material presented a higher hydrophobicity (water contact angle = 125 ± 3°) than nFe⁰ (33 ± 3°) and nFe⁰-FeS (60 ± 2°) materials (Figure 1h), consistent with our previous studies.^{34,36} These altered physicochemical properties would then change the reactivity and selectivity of materials toward aqueous TCE and TCE-NAPL, presenting different responses to the presence of PFASs, as described below.

3.2. Impacts of PFASs on the Reactivity and Selectivity of S-nFe⁰ Toward TCE and TCE-NAPL. The impacts of coexisting PFASs on the performance of materials for aqueous TCE degradation were first assessed to better understand the interactions between PFASs and materials. The degradation of aqueous TCE followed pseudo-first-order kinetics. The surface area normalized rates of aqueous TCE ($k_{SA,TCE}$) by S-nFe⁰ were 4–6 times higher than that by unmodified nFe⁰ (Figures 2a and S4) because sulfidized versions had a relatively lower impedance, faster electron transfer, and lower band gap.³² However, the coexistence of PFOA or PFOS inhibited the TCE degradation for all of the

materials studies, regardless of sulfidation and S speciation. PFOS inhibited the TCE degradation more significantly than PFOA for nFe⁰, while the inhibitory effects of PFOA and PFOS were similar for sulfidized versions. The inhibited reactivity might be caused by surface site occupation and steric hindrance after the adsorption of PFOA or PFOS (Figure S5). Although the adsorbed PFASs on nFe⁰ particles may improve their hydrophobicity and inhibit their aggregations through steric repulsions, the long carbon chains of PFASs may also reduce the reactivity by blocking active surface sites, similar as if nFe⁰ were coated with polymers.^{49,50} The main degradation product of aqueous TCE by nFe⁰, nFe⁰-FeS, and nFe⁰-FeS₂ was ethane (C₂H₆), ethylene (C₂H₄), and acetylene (C₂H₂), respectively (Figure 2c). This was because the H adsorption by Fe sites could be blocked by the nearby S sites,⁵¹ which in turn inhibited the hydrogenation of unsaturated hydrocarbons.⁵² While the surface adsorbed PFASs significantly increased the proportion of C₂H₄ generation by unmodified nFe⁰, they only slightly increased the proportions of C₂H₄ and C₂H₂ for TCE degradation by nFe⁰-FeS and nFe⁰-FeS₂, respectively. One possible reason was that the adsorption of PFASs more significantly increased the hydrophobicity of unmodified nFe⁰ than S-nFe⁰ (Figure S6), which tended to inhibit water reactivity and H adsorption for the hydrogenations of C₂H₄. This also indicates that the electron transfer and H adsorption abilities of S-nFe⁰ were likely dominated by S and its speciation rather than adsorbed PFASs.

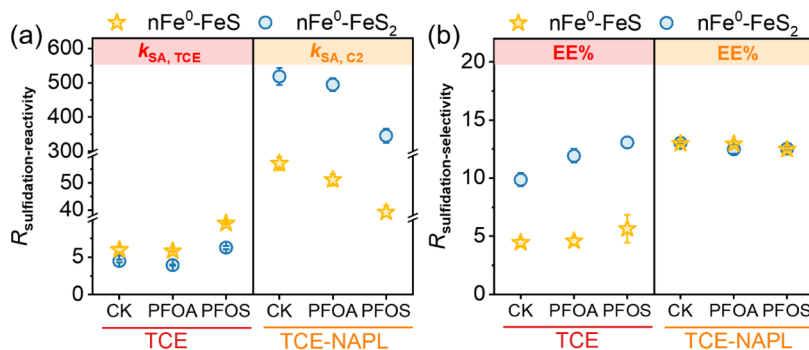


Figure 3. S-induced improvements in the (a) reactivity and (b) selectivity of aqueous TCE and TCE-NAPL degradation by materials. $R_{\text{sulfidation-reactivity}}$ denotes the ratios of TCE degradation ($k_{\text{SA}, \text{TCE}}$) or C_2 products generation rate ($k_{\text{SA}, \text{C}_2}$) by $S\text{-nFe}^0$ versus that by $n\text{Fe}^0$, and $R_{\text{sulfidation-selectivity}}$ denotes the ratios of electron efficiency (EE%) for TCE degradation by $S\text{-nFe}^0$ versus that by $n\text{Fe}^0$ (basic conditions: initial pH = 6.0 ± 0.2 , $T = 25 \pm 2^\circ\text{C}$, coexisting PFOA or PFOS = $100 \mu\text{g L}^{-1}$, iron material = 1.0 g L^{-1}).

The impacts of PFASs on the material reactivity and product distribution under the TCE-NAPL conditions were quite different compared to those under aqueous TCE conditions. Under these conditions, the initial rate of TCE degradation product generation (0–2 days) is more consistent with pseudozero-order kinetics. This pseudozero-order kinetics of TCE degradation under iron-limited conditions has been reported previously,^{37,42,53} and the initial rate of degradation product generation ($k_{\text{SA}, \text{C}_2}$) fitted by pseudozero-order kinetics was used to represent the degradation reactivity under TCE-NAPL conditions. Interestingly, a small amount of coexisting PFOA ($100 \mu\text{g L}^{-1}$) had a limited effect on $n\text{Fe}^0$ and $n\text{Fe}^0\text{-FeS}$ but promoted the degradation of TCE-NAPL by $n\text{Fe}^0\text{-FeS}_2$ (Figures 2b and S7). Higher concentrations of PFOA (500 and $1000 \mu\text{g L}^{-1}$) did not significantly change the product distribution and electron efficiency, except for a trend of slightly accelerated TCE-NAPL degradation compared to that of $100 \mu\text{g L}^{-1}$ PFOA (Figures S8 and S9). This may be because these concentrations were below the critical micelle concentration of PFOA and therefore presented limited effect. For the more hydrophobic coexisting PFOS, it promoted the degradation of TCE-NAPL by all these materials. The $n\text{Fe}^0\text{-FeS}_2$ material with higher hydrophobicity presented a relatively higher reactivity with TCE-NAPL than that with the $n\text{Fe}^0\text{-FeS}$ material. These trends were probably attributed to the favored contact between the materials and NAPL in the presence of PFASs, which could be easily enriched at the NAPL–water interface or distributed into the NAPL phase,^{15,18} as discussed later. The promotion effects of PFOS on the TCE-NAPL degradation were more significant than that of PFOA, regardless of the materials. In contrast, the presence of PFOS and PFOA did not change the product distribution of TCE-NAPL degradation by the $n\text{Fe}^0$, $n\text{Fe}^0\text{-FeS}$, and $n\text{Fe}^0\text{-FeS}_2$ materials (Figure 2d), where C_2H_4 (>89%), C_2H_2 (>95%), and C_2H_2 (>95%) were the dominant products, respectively. These values were much higher than that for the degradation of aqueous TCE (Figure 2c), consistent with a previous study.³⁷ The accumulation of unsaturated hydrocarbons under the TCE-NAPL condition indicates that the availability of electrons and H atoms per molecular for hydrogenation was quite low and the contact of materials with NAPL could be a potential factor to alter the reactivity and products distribution.

The improved reactivity of materials with TCE-NAPL is more beneficial if the materials are also selective for TCE reduction over water. The electron efficiency was calculated by quantifying the electrons consumed for H_2 , TCE, and their

degradation products to evaluate the selectivity of materials. The coexisting PFASs did not significantly affect the electron efficiency of materials for aqueous TCE degradation (Figure 2e), following a previously reported trend of $n\text{Fe}^0\text{-FeS}_2$ (46.4%) > $n\text{Fe}^0\text{-FeS}$ (20.9%) > $n\text{Fe}^0$ (4.7%), which largely depended on the hydrophobicity of materials.^{36,54} Similarly, the presence of PFASs also shows limited effects on the electron efficiency for TCE-NAPL degradation by the $n\text{Fe}^0$ and $S\text{-nFe}^0$ materials (Figure 2f), which was likely because TCE was in excess as compared to iron materials in the NAPL phase, NAPL–water interface, or TCE-saturated solution. Compared to aqueous TCE degradation by $n\text{Fe}^0\text{-FeS}$ and $n\text{Fe}^0\text{-FeS}_2$ materials, the electron efficiency of TCE-NAPL degradation greatly increased to 98.8% and 99.4%, respectively, probably because of favored material-NAPL contact and inhibited water reactivity (Figures S10 and S11). Although the electron efficiency of TCE-NAPL degradation by unmodified $n\text{Fe}^0$ also increased to 7.6%, this value was ~ 13 times lower than that by $S\text{-nFe}^0$ materials. Combined with the promoted reactivity by sulfidation, this result further indicates that $S\text{-nFe}^0$ was a much better version than $n\text{Fe}^0$ for NAPL remediation, as discussed below.

3.3. Comparison of S-Induced Performance Enhancements in the Presence of PFASs. The S-induced enhancements (R) defined as the ratios of the reactivity and selectivity for $S\text{-nFe}^0$ versus those for $n\text{Fe}^0$ were used to provide a more systematic comparison of the impacts of S speciation and PFASs. This will advance our understanding how S speciation in $S\text{-nFe}^0$ responds to the PFASs impacts on the materials' reactivity and selectivity, favoring rational design of $S\text{-nFe}^0$ materials for aqueous and nonaqueous TCE degradation in the presence of emerging PFASs. The R value of $n\text{Fe}^0\text{-FeS}$ ($R = 6$) was slightly higher than that of $n\text{Fe}^0\text{-FeS}_2$ ($R = 4.5$) for aqueous TCE degradation in the absence of PFASs (Figure 3a), consistent with the relatively faster electron transfer of $n\text{Fe}^0\text{-FeS}$ evaluated by electrochemical analysis (Figure 1g) and the lower hydrophobicity (Figure 1h) that could favor dechlorination via hydrogenolysis and hydrogenation. When PFOA coexisted, the R values of $n\text{Fe}^0\text{-FeS}$ and $n\text{Fe}^0\text{-FeS}_2$ were similar to those in the absence of PFASs, while these values stand out as higher in the presence of PFOS (9.5 and 6.3, respectively). This result suggests that the sulfidized version would be a much better choice than unmodified $n\text{Fe}^0$ in the presence of PFASs, especially in the case of PFASs with a relatively higher affinity (e.g., PFOS) toward the materials (Figure S5). However, these trends were opposite for TCE-

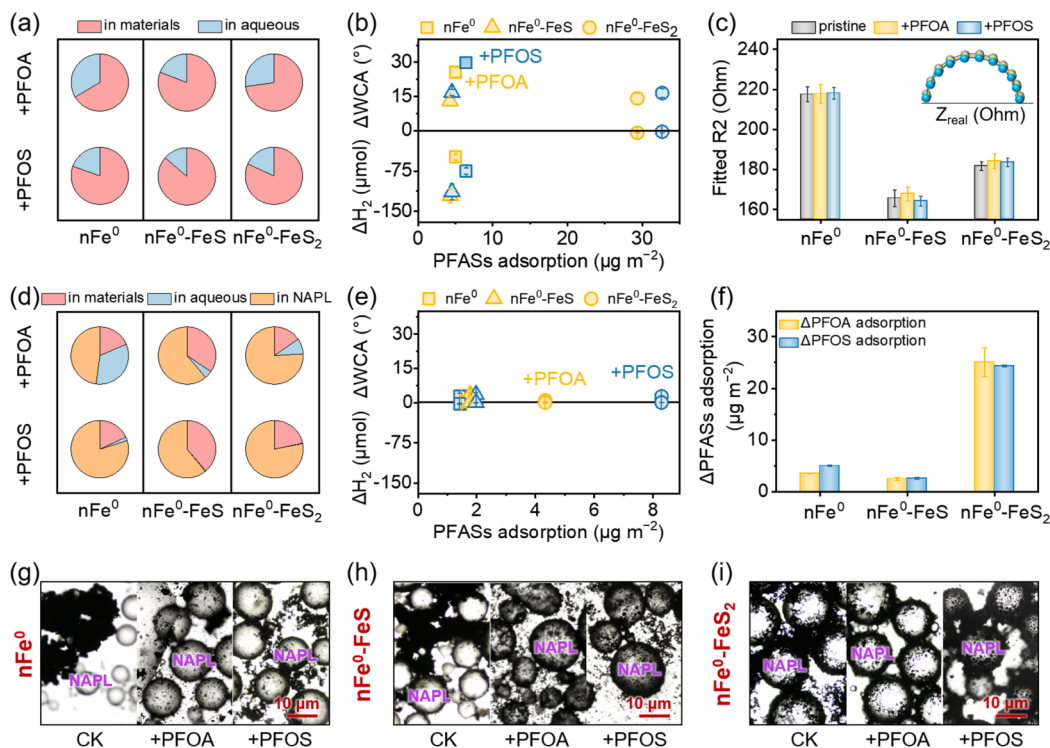


Figure 4. S speciation and PFASs impacted the physicochemical properties, reactivity, and mass transfer of materials. Distribution of PFAS after 8-day degradations of (a) aqueous TCE and (d) TCE-NAPL. Changes in water contact angle ($\Delta WCA = WCA_{\text{with PFASs}} - WCA_{\text{without PFASs}}$) and H_2 accumulation ($\Delta H_2 = H_2 \text{ with PFASs} - H_2 \text{ without PFASs}$) as a function of surface area normalized PFAS adsorption (Q_{SA}) after 8-day degradations of (b) aqueous TCE and (e) TCE-NAPL. (c) Fitted resistance from EIS data of materials before and after the adsorption of PFASs. (f) Changes in PFASs adsorption after 8-day degradations of aqueous TCE and TCE-NAPL ($\Delta \text{PFASs adsorption} = \text{PFASs adsorption in the aqueous TCE system} - \text{PFASs adsorption in the TCE-NAPL system}$). (g–i) S speciation and coexisting PFASs impacted mass transfer of materials assessed by optical microscopy images of material distribution at the NAPL–water interfaces (basic conditions: initial pH = 6.0 ± 0.2 , $T = 25 \pm 2^\circ\text{C}$, coexisting PFOA or PFOS = $100 \mu\text{g L}^{-1}$, iron material = 1.0 g L^{-1}).

NAPL degradation. The R values of nFe^0-FeS_2 ($R = 519$) in turn became higher than that of nFe^0-FeS ($R = 57$), which were 115.3-fold and 9.5-fold of those for aqueous TCE degradation, suggesting that nFe^0-FeS_2 held better promise for NAPL remediation compared to nFe^0-FeS and unmodified nFe^0 . Although coexisting PFOA and PFOS decreased the S-induced enhancement of reactivity with NAPL, the R values of nFe^0-FeS_2 ($R = 495$ and 346) were still much higher than those of nFe^0-FeS ($R = 51$ and 39).

The R values of electron efficiency were also compared to assess the impacts of S speciation and coexisting PFASs on the materials' selectivity toward TCE. The R values of nFe^0-FeS_2 were 10 for aqueous TCE degradation, and the presence of PFOA or PFOS had a limited effects on the R values ($R = 12$ and 13 , respectively). The R values of nFe^0-FeS ($R = 4.5$, 4.6 , and 5.6) were lower than these. While for TCE-NAPL degradation, the S speciation (FeS or FeS_2) and coexisting PFASs (PFOA or PFOS) did not significantly change the selectivity enhancement. This negligible effect implied that the phenomenon of TCE-NAPL outcompeting water for reactive sites was largely determined by the advantages of sulfidation (e.g., improved hydrophobicity and blocked H adsorption).^{55,56} The above results of material performance for aqueous TCE and TCE-NAPL degradation were likely because of the S speciation and PFASs impacted mass transfer of materials and their contact with NAPL, as discussed below.

3.4. Possible Mechanisms of PFASs- and S-Affected Degradation of TCE and TCE-NAPL

The PFASs distribu-

tion and their effects on materials' property-performance relationship were analyzed to reveal a possible mechanism of PFASs- and S-affected degradation of TCE and its NAPL version. The distributions of PFOA and PFOS in degradation systems were first quantified. In the aqueous TCE system, the majority of PFOA and PFOS (66.5–86.3%) was distributed in the solid phase (Figure 4a), i.e., being adsorbed on the iron materials. The adsorption of PFOS by the three materials was relatively higher than that of PFOA. Generally, electrostatic and hydrophobic interactions are often acquiesced to play important roles in the adsorption of PFASs,^{40,57,58} and long-chain PFASs (e.g., PFOS) with a high octanol–water partition coefficient may further acknowledge the hydrophobic interaction.^{59,60} The relatively lower adsorbed amount of PFASs onto nFe^0-FeS_2 compared to nFe^0-FeS was probably attributed to its ~ 7.5 times lower specific surface area (Figure S12). Thus, the adsorbed amount of PFASs was normalized by surface area (Q_{SA}) to rule out its impact, better understanding the unique roles of S species and coexisting PFASs in the materials' properties and reactivity. The Q_{SA} values of PFOA and PFOS by nFe^0-FeS_2 were 6–7 and 6–8 times higher than those of unmodified nFe^0 and nFe^0-FeS , respectively, which is in good agreement with their hydrophobicity (Figure 1h). The adsorbed PFASs improved the hydrophobicity of materials due to the hydrophobic nature of PFASs (Figures S6 and S13), which in turn inhibited the H_2 evolution by hydrophilic nFe^0 and nFe^0-FeS (Figure 4b) but did not present an obvious impact on the nFe^0-FeS_2 material that was already hydrophobic

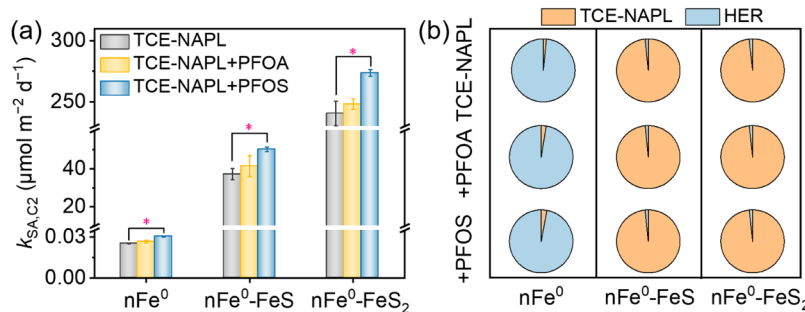


Figure 5. Impacts of S speciation and coexisting PFASs on the (a) reactivity and (b) selectivity of materials with TCE-NAPL in real groundwater (basic conditions: initial pH = 7.5 ± 0.2, T = 25 ± 2 °C, coexisting PFOA or PFOS = 100 µg L⁻¹, iron material = 1.0 g L⁻¹).

before the interaction with PFASs. In addition, the fitted charge transfer resistance suggests that adsorbing a small amount of PFAS had little effect on the overall electron transfer rates of the iron materials (Figure 4c).

These results indicated that the adsorption of PFOA and PFOS to the particles' surface improved its hydrophobicity and thus inhibited hydrogen evolution to some extent but did not passivate the materials if their surface reactive sites were accessible for target contaminants. However, the adsorption of PFOA/PFOS led by hydrophobic interaction tends to lay flat on the material surface, occupying part of the surface sites, but also diffusing laterally on the surface to form a certain thickness (a few nanometers) of aggregates/layered structures.^{61,62} Similar to other surfactants that are adsorbed on the material surface to hinder the diffusion of contaminants or to block the reaction site of the material,^{49,50} these aggregators would inevitably generate steric hindrance, which isolated aqueous TCE molecules from the surface reactive sites of materials and inhibited their reactions (Figure 2a). In addition, the PFASs adsorption on the surface of materials would inhibit their water reactivity, as described above (Figures 4b and S10).

While the surface adsorbed PFASs might induce steric hindrance to inhibit the TCE reduction in the aqueous TCE system, the situation was changed for the TCE-NAPL system. The PFASs were mainly distributed into the NAPL phase (Figure 4d), consistent with previous reports that PFASs could be easily enriched at the NAPL–water interface or distributed into the NAPL phase.^{15,18} This limited accumulation of PFASs on the materials surface led to much smaller changes in the hydrophobicity and H₂ evolution of materials (Figure 4e), compared to those in the aqueous TCE system. The Q_{SA} values of PFASs on the hydrophobic nFe⁰-FeS₂ material (4.3 and 8.3 µg m⁻²) were still higher than those on the hydrophilic nFe⁰ and nFe⁰-FeS materials (1.4–2.0 µg m⁻²). In addition, the concentrations of aqueous PFASs decreased faster in the TCE-NAPL system than in the aqueous TCE system (Figure S14). The discrepancies of Q_{SA} values between the aqueous TCE and TCE-NAPL systems for the hydrophobic nFe⁰-FeS₂ material (~25 µg m⁻²) were also much higher than those for the hydrophilic nFe⁰ (~5 µg m⁻²) and nFe⁰-FeS (~3 µg m⁻²) materials (Figure 4f). These results further confirmed that PFASs tended to accumulate in the NAPL phase rather than onto the materials even with a hydrophobic surface, also indicating that the interactions of materials with coexisting PFASs and the favorable mass transfer of PFASs might affect the distribution of materials in the NAPL degradation system.

NAPL drop interactions with materials in the absence and presence of PFASs were further investigated to provide another proof. Optical microscope images of NAPL–water interfaces

(Figure 4g) show that the most nFe⁰ particles were aggregated that being separated from NAPL drops in the absence of PFASs, compared to being enriched at the NAPL–water interface in the presence of PFASs. This indicates that the coexisting PFASs could help the contact between materials and NAPL, favoring the reductions, as shown in Figure 2b. This phenomenon was also presented for the S-nFe⁰ materials (Figure 4h,i), where the hydrophobic nFe⁰-FeS₂ material enriched more at the NAPL–water interface or into the NAPL phase than the hydrophilic nFe⁰-FeS material. This was probably because both PFASs and hydrophobic materials tended to accumulate at the NAPL–water interface,^{22,45,63,64} and the materials adsorbed with PFASs were also readily transferred to the NAPL phase or enriched at the NAPL–water interface. Compared with other surfactants that often enhance NAPL remediation by promoting NAPL mobilization and increasing NAPL dissolution through micelles,⁶⁵ the high surface activity of PFASs might be the reason for its ability to mobilize the transportation of PFASs adsorbed materials at low concentrations (below the critical micelle concentration). PFOS presented a stronger promotion on the accumulation of materials than PFOA, similar to their impacts on the materials' reactivity (Figure 2a,b). Generally, the headgroup of PFOA and PFOS played an important role in their interfacial behaviors, because it affects not only their hydrophobicity but also their protonation state in solution, thus affecting their adsorption in the solid phase, NAPL–water interface distribution, and NAPL phase partitioning.^{16,18} Based on the above phenomena, the possible mechanism of PFASs promoting TCE-NAPL degradation was proposed. The surface adsorbed PFOA or PFOS would help the materials to be concentrated at the NAPL–water interface, similar to the distribution tendency of PFOA and PFOS. Also, the hydrophobicity of materials would help this distribution of materials. Once the majority of PFASs was distributed in the NAPL phase, the re-exposed materials that well contact with NAPL at the NAPL–water interface would promote the TCE degradation, where TCE outcompeted water for electrons from materials (i.e., high selectivity).

3.5. Materials Performance Under Environmentally Relevant Groundwater Conditions. The impacts of S speciation and coexisting PFASs on the material performance were tested in real groundwater to evaluate their application potential for the TCE-NAPL remediation in the presence of PFASs. While unmodified nFe⁰ became inert (Figures 5a and S15), nFe⁰-FeS and nFe⁰-FeS₂ materials were still reactive with TCE-NAPL in real groundwater, and the coexisting PFASs tended to promote the TCE-NAPL degradation. The slightly slower C₂ product generation (Figure S15) and H₂ evolution

(Figure S16) in real groundwater compared to that in DI water were likely attributed to the presence of dissolved ions and organic matter, as well as the relatively higher pH of groundwater ($\text{pH} = 7.5 \pm 0.2$) that might passivate the materials to some extent.^{66–69} The groundwater matrix did not change the product distribution of TCE-NAPL degradation by $\text{nFe}^0\text{-FeS}$ and $\text{nFe}^0\text{-FeS}_2$ materials (Figure S15), where C_2H_2 was the primary dechlorination product. Moreover, these two S-nFe^0 materials still presented high electron efficiencies (>98%) that were not significantly affected by the small amount of coexisting PFOA or PFOS (Figure 5b). This high electron efficiency indicates a promising potential of S-nFe^0 materials in field applications because most electrons from Fe^0 would be utilized for the reduction of target contaminant, despite the TCE-NAPL degradation needs a relatively longer time compared to that in DI water.

4. ENVIRONMENTAL IMPLICATIONS

This study reveals that the interactions of S-nFe^0 particles with a small amount of coexisting PFASs can change the materials' hydrophobicity and contact with TCE and its NAPL version, affecting the dechlorination reactivity and selectivity. The impacts of coexisting PFASs can be altered by S speciation in S-nFe^0 materials. The valuable information provided here will promote the rational design of groundwater remediation agents in the presence of emerging contaminants, e.g., PFASs. The coexisting PFASs could slower the aqueous TCE degradation with limited impact on the electron efficiency, despite improving the materials' hydrophobicity without affecting the overall rates of electron transfer. This indicates that the dechlorination of TCE in the aqueous phase by S-nFe^0 materials could be sterically hindered by the surface adsorbed PFASs, and increasing materials' hydrophobicity does not necessarily improve their TCE reactivity and selectivity if the mass transfer was blocked. In contrast, the coexisting PFASs accelerated the dechlorination of TCE-NAPL due to improved enrichments of PFASs and materials at the NAPL–water interfaces or even into the NAPL phases, allowing sufficient contact between materials and NAPL. While the detailed distribution of PFASs and relevant fundamental insights merit exploring under varied NAPL conditions, these results indicate that a high affinity with PFASs could probably inhibit the materials' reactivity with aqueous TCE but promote their reactivity with TCE-NAPL, and we need to rationally design materials for different TCE remediation scenarios.

Three studied materials without or with different S species presented different distributions of PFASs and materials in the TCE-NAPL systems, indicating that the hydrophobicity and electron transfer induced by impregnating materials with controllable S speciation remain important factors in determining the reactivity and selectivity toward aqueous TCE and TCE-NAPL. The comparisons of S-induced performance enhancements in the presence of PFASs suggest that $\text{nFe}^0\text{-FeS}_2$ holds a better promise toward NAPL remediation compared to unmodified nFe^0 and $\text{nFe}^0\text{-FeS}$. In addition, PFOS with a higher hydrophobicity and octanol–water partition coefficient exhibited stronger inhibition on aqueous TCE degradation and promotion of TCE-NAPL degradation, compared to PFOA. It may help us to estimate the relative impacts of coexisting PFASs, e.g., long-chain PFASs versus short-chain PFASs or even emerging PFASs; however, this needs further evaluation. Also, more conclusive evidence on how coexisting PFASs affect the transportation of iron

nanomaterials during the remediation process will further advance our understanding of the PFASs impacts on materials' reactivity, guiding the design of iron nanomaterials.

■ ASSOCIATED CONTENT

SI Supporting Information

The Supporting Information is available free of charge at <https://pubs.acs.org/doi/10.1021/acs.est.4c04466>.

Chemicals and materials, methods for mass transfer and characterization of materials, methods for analysis of TCE degradation products and PFASs, supporting figures and tables (PDF)

■ AUTHOR INFORMATION

Corresponding Author

Jiang Xu – College of Environmental and Resource Sciences, Zhejiang University, Hangzhou 310058, China; Zhejiang Provincial Key Laboratory of Organic Pollution Process and Control, Zhejiang University, Hangzhou 310058, China;
✉ orcid.org/0000-0003-0369-4848; Email: xujiang6@zju.edu.cn

Authors

Du Chen – College of Environmental and Resource Sciences, Zhejiang University, Hangzhou 310058, China

Xiaohong Hu – College of Environmental and Resource Sciences, Zhejiang University, Hangzhou 310058, China

Chaochuang Chen – College of Environmental and Resource Sciences, Zhejiang University, Hangzhou 310058, China

Yiman Gao – College of Environmental and Resource Sciences, Zhejiang University, Hangzhou 310058, China

Qianhai Zhou – College of Environmental and Resource Sciences, Zhejiang University, Hangzhou 310058, China

Xia Feng – College of Environmental and Resource Sciences, Zhejiang University, Hangzhou 310058, China

Xinhua Xu – College of Environmental and Resource Sciences, Zhejiang University, Hangzhou 310058, China;
✉ orcid.org/0000-0001-7139-1246

Daohui Lin – College of Environmental and Resource Sciences, Zhejiang University, Hangzhou 310058, China; Zhejiang Provincial Key Laboratory of Organic Pollution Process and Control, Zhejiang University, Hangzhou 310058, China;
✉ orcid.org/0000-0002-9662-7195

Complete contact information is available at:
<https://pubs.acs.org/10.1021/acs.est.4c04466>

Notes

The authors declare no competing financial interest.

■ ACKNOWLEDGMENTS

This work was supported by the National Natural Science Foundation of China (22306157, U21A20163, and 22206165), National Key Research and Development Program of China (2021YFA1202700 and 2022YFC3203403), and the Key Research and Development Program of Zhejiang Province (2024C03228).

■ REFERENCES

- (1) McGuire, M. E.; Schaefer, C.; Richards, T.; Backe, W. J.; Field, J. A.; Houtz, E.; Sedlak, D. L.; Guelfo, J. L.; Wunsch, A.; Higgins, C. P. Evidence of Remediation-Induced Alteration of Subsurface Poly- and

- Perfluoroalkyl Substance Distribution at a Former Firefighter Training Area. *Environ. Sci. Technol.* **2014**, *48* (12), 6644–6652.
- (2) Moody, C. A.; Hebert, G. N.; Strauss, S. H.; Field, J. A. Occurrence and Persistence of Perfluoroctanesulfonate and other Perfluorinated Surfactants in Groundwater at a Fire-Training Area at Wurtsmith Air Force Base, Michigan, USA. *J. Environ. Monit.* **2003**, *5* (2), 341–345.
- (3) Guelfo, J. L.; Higgins, C. P. Subsurface Transport Potential of Perfluoroalkyl Acids at Aqueous Film-Forming Foam (AFFF)-Impacted Sites. *Environ. Sci. Technol.* **2013**, *47* (9), 4164–4171.
- (4) Houtz, E. F.; Higgins, C. P.; Field, J. A.; Sedlak, D. L. Persistence of Perfluoroalkyl Acid Precursors in AFFF-Impacted Groundwater and Soil. *Environ. Sci. Technol.* **2013**, *47* (15), 8187–8195.
- (5) Liao, S.; Saleeba, Z.; Bryant, J. D.; Abriola, L. M.; Pennell, K. D. Influence of Aqueous Film Forming Foams on the Solubility and Mobilization of Non-Aqueous Phase Liquid Contaminants in Quartz Sands. *Water Res.* **2021**, *195*, 116975.
- (6) Moody, C. A.; Field, J. A. Perfluorinated Surfactants and the Environmental Implications of Their Use in Fire-Fighting Foams. *Environ. Sci. Technol.* **2000**, *34* (18), 3864–3870.
- (7) Schultz, M. M.; Barofsky, D. F.; Field, J. A. Quantitative Determination of Fluorotelomer Sulfonates in Groundwater by LC MS/MS. *Environ. Sci. Technol.* **2004**, *38* (6), 1828–1835.
- (8) Dauchy, X.; Boiteux, V.; Bach, C.; Rosin, C.; Munoz, J. F. Per- and Polyfluoroalkyl Substances in Firefighting Foam Concentrates and Water Samples Collected near Sites Impacted by the Use of These Foams. *Chemosphere* **2017**, *183*, 53–61.
- (9) Awad, E.; Zhang, X.; Bhavsar, S. P.; Petro, S.; Crozier, P. W.; Reiner, E. J.; Fletcher, R.; Tittlemier, S. A.; Braekevelt, E. Long-Term Environmental Fate of Perfluorinated Compounds after Accidental Release at Toronto Airport. *Environ. Sci. Technol.* **2011**, *45* (19), 8081–8089.
- (10) Bräunig, J.; Baduel, C.; Heffernan, A.; Rotander, A.; Donaldson, E.; Mueller, J. F. Fate and Redistribution of Perfluoroalkyl Acids Through AFFF-Impacted Groundwater. *Sci. Total Environ.* **2017**, *596*–597, 360–368.
- (11) Cao, L.; Xu, W.; Wan, Z.; Li, G.; Zhang, F. Occurrence of PFASs and its Effect on Soil Bacteria at a Fire-Training Area Using PFOS-Restricted Aqueous Film-Forming Foams. *iScience* **2022**, *25* (4), 104084.
- (12) Tang, Z.; Song, X.; Xu, M.; Yao, J.; Ali, M.; Wang, Q.; Zeng, J.; Ding, X.; Wang, C.; Zhang, Z.; Liu, X. Effects of Co-occurrence of PFASs and Chlorinated Aliphatic Hydrocarbons on Microbial Communities in Groundwater: A Field Study. *J. Hazard. Mater.* **2022**, *435*, 128969.
- (13) Harding-Marjanovic, K. C.; Yi, S.; Weathers, T. S.; Sharp, J. O.; Sedlak, D. L.; Alvarez-Cohen, L. Effects of Aqueous Film-Forming Foams (AFFFs) on Trichloroethene (TCE) Dechlorination by a Dehalococcoides mccartyi-Containing Microbial Community. *Environ. Sci. Technol.* **2016**, *50* (7), 3352–3361.
- (14) Brusseau, M. L.; Yan, N.; Glubt, S. V.; Wang, Y.; Chen, W.; Lyu, Y.; Dungan, B.; Carroll, K. C.; Holguin, F. O. Comprehensive Retention Model for PFAS Transport in Subsurface Systems. *Water Res.* **2019**, *148*, 41–50.
- (15) Brusseau, M. L. Assessing the Potential Contributions of Additional Retention Processes to PFAS Retardation in the Subsurface. *Sci. Total Environ.* **2018**, *613*–614, 176–185.
- (16) Liao, S.; Arshadi, M.; Woodcock, M. J.; Saleeba, Z.; Pinchbeck, D.; Liu, C.; Capiro, N. L.; Abriola, L. M.; Pennell, K. D. Influence of Residual Nonaqueous-Phase Liquids (NAPLs) on the Transport and Retention of Perfluoroalkyl Substances. *Environ. Sci. Technol.* **2022**, *56* (12), 7976–7985.
- (17) Liu, H.; Guo, Z.; Zhu, Y.; Glubt, S. V.; Brusseau, M. L. The Influence of NAPL Distribution on the Transport of PFOS in Co-contaminated Media. *J. Hazard. Mater.* **2024**, *462*, 132794.
- (18) Glubt, S. V.; Brusseau, M. L. Contribution of Nonaqueous-Phase Liquids to the Retention and Transport of Per- and Polyfluoroalkyl Substances (PFAS) in Porous Media. *Environ. Sci. Technol.* **2021**, *55* (6), 3706–3715.
- (19) McKenzie, E. R.; Siegrist, R. L.; McCray, J. E.; Higgins, C. P. The Influence of a Non-Aqueous Phase Liquid (NAPL) and Chemical Oxidant Application on Perfluoroalkyl Acid (PFAA) Fate and Transport. *Water Res.* **2016**, *92*, 199–207.
- (20) Hakimabadi, S. G.; Taylor, A.; Pham, A. L.-T. Factors Affecting the Adsorption of Per- and Polyfluoroalkyl Substances (PFAS) by Colloidal Activated Carbon. *Water Res.* **2023**, *242*, 120212.
- (21) Quinn, J.; Geiger, C.; Clausen, C.; Brooks, K.; Coon, C.; O'Hara, S.; Krug, T.; Major, D.; Yoon, W.-S.; Gavaskar, A.; Holdsworth, T. Field Demonstration of DNAPL Dehalogenation Using Emulsified Zero-Valent Iron. *Environ. Sci. Technol.* **2005**, *39* (5), 1309–1318.
- (22) Phenrat, T.; Kumloet, I. Electromagnetic Induction of Nanoscale Zerovalent Iron Particles Accelerates the Degradation of Chlorinated Dense Non-Aqueous Phase Liquid: Proof of Concept. *Water Res.* **2016**, *107*, 19–28.
- (23) Zhang, T.; Lowry, G. V.; Capiro, N. L.; Chen, J.; Chen, W.; Chen, Y.; Dionysiou, D. D.; Elliott, D. W.; Ghoshal, S.; Hofmann, T.; Hsu-Kim, H.; Hughes, J.; Jiang, C.; Jiang, G.; Jing, C.; Kavanaugh, M.; Li, Q.; Liu, S.; Ma, J.; Pan, B.; Phenrat, T.; Qu, X.; Quan, X.; Saleh, N.; Vikesland, P. J.; Wang, Q.; Westerhoff, P.; Wong, M. S.; Xia, T.; Xing, B.; Yan, B.; Zhang, L.; Zhou, D.; Alvarez, P. J. J. In Situ Remediation of Subsurface Contamination: Opportunities and Challenges for Nanotechnology and Advanced Materials. *Environ. Sci.: Nano* **2019**, *6* (5), 1283–1302.
- (24) Garcia, A. N.; Zhang, Y.; Ghoshal, S.; He, F.; O'Carroll, D. M. Recent Advances in Sulfidated Zerovalent Iron for Contaminant Transformation. *Environ. Sci. Technol.* **2021**, *55* (13), 8464–8483.
- (25) Rajajayavel, S. R.; Ghoshal, S. Enhanced Reductive Dechlorination of Trichloroethylene by Sulfidated Nanoscale Zerovalent Iron. *Water Res.* **2015**, *78*, 144–153.
- (26) Xu, J.; Li, H.; Lowry, G. V. Sulfidized Nanoscale Zero-Valent Iron: Tuning the Properties of This Complex Material for Efficient Groundwater Remediation. *Acc. Mater. Res.* **2021**, *2* (6), 420–431.
- (27) Xu, J.; Chen, C.; Hu, X.; Chen, D.; Bland, G.; Wielinski, J.; Kaegi, R.; Lin, D.; Lowry, G. V. Particle-Scale Understanding of Arsenic Interactions with Sulfidized Nanoscale Zerovalent Iron and Their Impacts on Dehalogenation Reactivity. *Environ. Sci. Technol.* **2023**, *57* (51), 21917–21926.
- (28) Zhang, Y.; Ozcer, P.; Ghoshal, S. A Comprehensive Assessment of the Degradation of C1 and C2 Chlorinated Hydrocarbons by Sulfidated Nanoscale Zerovalent Iron. *Water Res.* **2021**, *201*, 117328.
- (29) Fan, D.; Lan, Y.; Tratnyek, P. G.; Johnson, R. L.; Filip, J.; O'Carroll, D. M.; Garcia, A. N.; Agrawal, A. Sulfidation of Iron-Based Materials: A Review of Processes and Implications for Water Treatment and Remediation. *Environ. Sci. Technol.* **2017**, *51* (22), 13070–13085.
- (30) Su, Y.; Jassby, D.; Song, S.; Zhou, X.; Zhao, H.; Filip, J.; Petala, E.; Zhang, Y. Enhanced Oxidative and Adsorptive Removal of Diclofenac in Heterogeneous Fenton-like Reaction with Sulfide Modified Nanoscale Zerovalent Iron. *Environ. Sci. Technol.* **2018**, *52* (11), 6466–6475.
- (31) Li, J.; Zhang, X.; Sun, Y.; Liang, L.; Pan, B.; Zhang, W.; Guan, X. Advances in Sulfidation of Zerovalent Iron for Water Decontamination. *Environ. Sci. Technol.* **2017**, *51* (23), 13533–13544.
- (32) Xu, J.; Avellan, A.; Li, H.; Liu, X.; Noel, V.; Lou, Z.; Wang, Y.; Kaegi, R.; Henkelman, G.; Lowry, G. V. Sulfur Loading and Speciation Control the Hydrophobicity, Electron Transfer, Reactivity, and Selectivity of Sulfidized Nanoscale Zerovalent Iron. *Adv. Mater.* **2020**, *32* (17), 1906910.
- (33) Chen, D.; Hu, X.; Chen, C.; Lin, D.; Xu, J. Tailoring Fe⁰ Nanoparticles via Lattice Engineering for Environmental Remediation. *Environ. Sci. Technol.* **2023**, *57* (45), 17178–17188.
- (34) Hu, X.; Chen, C.; Chen, D.; Noel, V.; Oji, H.; Ghoshal, S.; Lowry, G. V.; Tratnyek, P. G.; Lin, D.; Zhu, L.; Xu, J. Lattice Engineered Nanoscale Fe⁰ for Selective Reductions. *Nature Water* **2024**, *2*, 84–92.

- (35) White, J. J.; Hinsch, J. J.; Wu, Z.; Tian, Y.; Bennett, W. W.; Wang, Y. Sulfidation Impacts on the Hydrophobicity of Stepped Iron Surfaces. *Adv. Energy Sustainability Res.* **2023**, *4*, 2300055.
- (36) Xu, J.; Avellan, A.; Li, H.; Clark, E. A.; Henkelman, G.; Kaegi, R.; Lowry, G. V. Iron and Sulfur Precursors Affect Crystalline Structure, Speciation, and Reactivity of Sulfidized Nanoscale Zerovalent Iron. *Environ. Sci. Technol.* **2020**, *54* (20), 13294–13303.
- (37) Xu, J.; Cao, Z.; Zhou, H.; Lou, Z.; Wang, Y.; Xu, X.; Lowry, G. V. Sulfur Dose and Sulfidation Time Affect Reactivity and Selectivity of Post-Sulfidized Nanoscale Zerovalent Iron. *Environ. Sci. Technol.* **2019**, *53* (22), 13344–13352.
- (38) Cao, Z.; Li, H.; Lowry, G. V.; Shi, X.; Pan, X.; Xu, X.; Henkelman, G.; Xu, J. Unveiling the Role of Sulfur in Rapid Defluorination of Florfenicol by Sulfidized Nanoscale Zero-Valent Iron in Water under Ambient Conditions. *Environ. Sci. Technol.* **2021**, *55*, 2628–2638.
- (39) Cao, Z.; Li, H.; Xu, X.; Xu, J. Correlating Surface Chemistry and Hydrophobicity of Sulfidized Nanoscale Zerovalent Iron with its Reactivity and Selectivity for Denitrification and Dechlorination. *Chem. Eng. J.* **2020**, *394*, 124876.
- (40) Zhang, Y.; Zhi, Y.; Liu, J.; Ghoshal, S. Sorption of Perfluoroalkyl Acids to Fresh and Aged Nanoscale Zerovalent Iron Particles. *Environ. Sci. Technol.* **2018**, *52* (11), 6300–6308.
- (41) Fan, D.; O'Brien Johnson, G.; Tratnyek, P. G.; Johnson, R. L. Sulfidation of Nano Zerovalent Iron (nZVI) for Improved Selectivity During In-Situ Chemical Reduction (ISCR). *Environ. Sci. Technol.* **2016**, *50* (17), 9558–9565.
- (42) He, F.; Li, Z.; Shi, S.; Xu, W.; Sheng, H.; Gu, Y.; Jiang, Y.; Xi, B. Dechlorination of Excess Trichloroethene by Bimetallic and Sulfidated Nanoscale Zero-Valent Iron. *Environ. Sci. Technol.* **2018**, *52* (15), 8627–8637.
- (43) Xiao, S.; Jin, Z.; Dong, H.; Xiao, J.; Li, Y.; Li, L.; Li, R.; Chen, J.; Tian, R.; Xie, Q. A Comparative Study on the Physicochemical Properties, Reactivity and Long-Term Performance of Sulfidized Nanoscale Zerovalent Iron Synthesized with Different Kinds of Sulfur Precursors and Procedures in Simulated Groundwater. *Water Res.* **2022**, *212*, 118097.
- (44) Bhattacharjee, S.; Ghoshal, S. Optimal Design of Sulfidated Nanoscale Zerovalent Iron for Enhanced Trichloroethene Degradation. *Environ. Sci. Technol.* **2018**, *52* (19), 11078–11086.
- (45) Bhattacharjee, S.; Ghoshal, S. Phase Transfer of Palladized Nanoscale Zerovalent Iron for Environmental Remediation of Trichloroethene. *Environ. Sci. Technol.* **2016**, *50* (16), 8631–8639.
- (46) Meng, F.; Xu, J.; Dai, H.; Yu, Y.; Lin, D. Even Incorporation of Nitrogen into Fe⁰ Nanoparticles as Crystalline Fe₄N for Efficient and Selective Trichloroethylene Degradation. *Environ. Sci. Technol.* **2022**, *56* (7), 4489–4497.
- (47) Van Zeghbroeck, B. Principles of Semiconductor Devices. In *The Oxford Series in Electrical and Computer Engineering*, University of Colorado, 2011.
- (48) Xu, Y.; Schoonen, M. A. A. The Absolute Energy Positions of Conduction and Valence Bands of Selected Semiconducting Minerals. *Am. Mineral.* **2000**, *85* (3–4), 543–556.
- (49) Phenrat, T.; Liu, Y.; Tilton, R. D.; Lowry, G. V. Adsorbed Polyelectrolyte Coatings Decrease Fe⁰ Nanoparticle Reactivity with TCE in Water: Conceptual Model and Mechanisms. *Environ. Sci. Technol.* **2009**, *43* (5), 1507–1514.
- (50) Bhattacharjee, S.; Basnet, M.; Tufenkiji, N.; Ghoshal, S. Effects of Rhamnolipid and Carboxymethylcellulose Coatings on Reactivity of Palladium-Doped Nanoscale Zerovalent Iron Particles. *Environ. Sci. Technol.* **2016**, *50* (4), 1812–1820.
- (51) Cao, Z.; Xu, J.; Li, H.; Ma, T.; Lou, L.; Henkelman, G.; Xu, X. Dechlorination and Defluorination Capability of Sulfidized Nanoscale Zerovalent Iron with Suppressed Water Reactivity. *Chem. Eng. J.* **2020**, *400*, 125900.
- (52) Cao, Z.; Li, H.; Zhang, S.; Hu, Y.; Xu, J.; Xu, X. Properties and Reactivity of Sulfidized Nanoscale Zero-Valent Iron Prepared with Different Borohydride Amounts. *Environ. Sci.: Nano* **2021**, *8* (9), 2607–2617.
- (53) Gu, Y.; Wang, B.; He, F.; Bradley, M. J.; Tratnyek, P. G. Mechanochemically Sulfidated Microscale Zero Valent Iron: Pathways, Kinetics, Mechanism, and Efficiency of Trichloroethylene Dechlorination. *Environ. Sci. Technol.* **2017**, *51* (21), 12653–12662.
- (54) Xu, J.; Wang, Y.; Weng, C.; Bai, W.; Jiao, Y.; Kaegi, R.; Lowry, G. V. Reactivity, Selectivity, and Long-Term Performance of Sulfidized Nanoscale Zerovalent Iron with Different Properties. *Environ. Sci. Technol.* **2019**, *53* (10), 5936–5945.
- (55) Burke, M. L.; Madix, R. J. Hydrogen on Pd(100)-S: The Effect of Sulfur on Precursor Mediated Adsorption and Desorption. *Surf. Sci.* **1990**, *237*, 1–19.
- (56) Bartholomew, C. H.; Agrawal, P. K.; Katzer, J. R. Sulfur Poisoning of Metals. In *Adv. Catal.*, Eley, D. D.; Pines, H.; Weisz, P. B., Ed.; Academic Press, 1982; Vol. 31, pp. 135242.
- (57) Wang, M.; Orr, A. A.; Jakubowski, J. M.; Bird, K. E.; Casey, C. M.; Hearon, S. E.; Tamamis, P.; Phillips, T. D. Enhanced Adsorption of Per- and Polyfluoroalkyl Substances (PFAS) by Edible, Nutrient-Amended Montmorillonite Clays. *Water Res.* **2021**, *188*, 116534.
- (58) Gagliano, E.; Sgroi, M.; Falciglia, P. P.; Vagliassindi, F. G. A.; Roccaro, P. Removal of Poly- and Perfluoroalkyl Substances (PFAS) from Water by Adsorption: Role of PFAS Chain Length, Effect of Organic Matter and Challenges in Adsorbent Regeneration. *Water Res.* **2020**, *171*, 115381.
- (59) Dong, Q.; Min, X.; Zhao, Y.; Wang, Y. Adsorption of Per- and Polyfluoroalkyl Substances (PFAS) by Ionic Liquid-modified Clays: Effect of Clay Composition and PFAS Structure. *J. Colloid Interface Sci.* **2024**, *654*, 925–934.
- (60) Park, M.; Wu, S.; Lopez, I. J.; Chang, J. Y.; Karanfil, T.; Snyder, S. A. Adsorption of Perfluoroalkyl Substances (PFAS) in Groundwater by Granular Activated Carbons: Roles of Hydrophobicity of PFAS and Carbon Characteristics. *Water Res.* **2020**, *170*, 115364.
- (61) Mohona, T. M.; Ye, Z.; Dai, N.; Nalam, P. C. Adsorption Behavior of Long-Chain Perfluoroalkyl Substances on Hydrophobic Surface: A Combined Molecular Characterization and Simulation Study. *Water Res.* **2023**, *239*, 120074.
- (62) Luft, C. M.; Schutt, T. C.; Shukla, M. K. Properties and Mechanisms for PFAS Adsorption to Aqueous Clay and Humic Soil Components. *Environ. Sci. Technol.* **2022**, *56* (14), 10053–10061.
- (63) Brusseau, M. L. Examining the Robustness and Concentration Dependency of PFAS Air-Water and NAPL-Water Interfacial Adsorption Coefficients. *Water Res.* **2021**, *190*, 116778.
- (64) Phenrat, T.; Fagerlund, F.; Illangasekare, T.; Lowry, G. V.; Tilton, R. D. Polymer-Modified Fe⁰ Nanoparticles Target Entrapped NAPL in Two Dimensional Porous Media: Effect of Particle Concentration, NAPL Saturation, and Injection Strategy. *Environ. Sci. Technol.* **2011**, *45* (14), 6102–6109.
- (65) Liu, J. W.; Wei, K. H.; Xu, S. W.; Cui, J.; Ma, J.; Xiao, X. L.; Xi, B. D.; He, X. S. Surfactant-Enhanced Remediation of Oil-Contaminated Soil and Groundwater: A Review. *Sci. Total Environ.* **2021**, *756*, 144142.
- (66) Gu, Y.; Gong, L.; Qi, J.; Cai, S.; Tu, W.; He, F. Sulfidation Mitigates the Passivation of Zero Valent Iron at Alkaline pHs: Experimental Evidences and Mechanism. *Water Res.* **2019**, *159*, 233–241.
- (67) Bae, S.; Hanna, K. Reactivity of Nanoscale Zero-Valent Iron in Unbuffered Systems: Effect of pH and Fe(II) Dissolution. *Environ. Sci. Technol.* **2015**, *49* (17), 10536–10543.
- (68) Song, H.; Carraway, E. R. Reduction of Chlorinated Ethanes by Nanosized Zero-Valent Iron: Kinetics, Pathways, and Effects of Reaction Conditions. *Environ. Sci. Technol.* **2005**, *39* (16), 6237–6245.
- (69) Zhang, L.; Zhang, Y.; Gao, X.; Xu, C. Insights on the Effects of pH and Fe(II) Regeneration during the Chromate Sequestration by Sulfidated Zero-Valent Iron. *Chem. Eng. J.* **2019**, *378*, 122115.